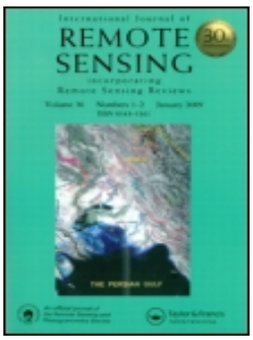

International Journal of Remote Sensing

ISSN: 0143-1161 (Print) 1366-5901 (Online) Journal homepage: http://www.tandfonline.com/loi/tres20

Determination of surface reflectance from raw hyperspectral data without simultaneous ground data measurements: A case study of the GER 63-channel sensor data acquired over Naan, Israel

E. Ben-Dor & N. Levin

To cite this article: E. Ben-Dor & N. Levin (2000) Determination of surface reflectance from raw hyperspectral data without simultaneous ground data measurements: A case study of the GER 63-channel sensor data acquired over Naan, Israel, International Journal of Remote Sensing, 21:10, 2053-2074, DOI: 10.1080/01431160050021295

To link to this article: https://doi.org/10.1080/01431160050021295

INT. J. REMOTE SENSING, 2000, VOL. 21, NO. 10, 2053–2074

Determination of surface reflectance from raw hyperspectral data without simultaneous ground data measurements: a case study of the GER 63-channel sensor data acquired over Naan, Israel

E. BEN-DOR† and N. LEVIN

Department of Geography, Tel-Aviv University, Ramat-Aviv Tel-Aviv, P.O. Box 39040, Israel 69978

(*Received 10 October 1997; in final form 29 July 1998*)

Abstract. Raw hyperspectral data that were acquired over Israel in 1989 by the GER 63-channel scanner were processed to provide surface reflectances seven years after the flight. Because no ground data measurements were available for the time of the flight, four atmospheric correction methods were applied: Atmospheric REMoval program (ATREM), Internal Average Relative Reflectance (IARR), Flat Field (FF) and Empirical Line (EL). Neither the ATREM program, which is an atmospheric model-based method, nor the IARR or the FF techniques, which are scene-dependent methods, were able to provide reasonable results. Whereas the failure of the ATREM program was probably because of a sensor's radiometric problem in the visible (VIS) region, the IARR and FF methods failed because of the relative complexity of the landscape. Of the three EL combinations examined, only one was able to convert the raw digital data into reasonable apparent reflectance information. Processing the data with this combination resulted in a good match between the spectra of selected targets taken from the image and their associated laboratory spectra. Samples, which were collected seven years after the actual flight, were used to assess the ability of each EL correction method to remove atmospheric attenuation. It was concluded that when working with such so-called 'hopeless' data, in order to obtain reasonable results, several combinations of the EL method need to be applied. The results of each method should then be judged, from both a spectral and a spatial perspective, against a separate set of samples, which were not a part of the correction procedure. In this case study, the spectral examination involved 20 samples, and the spatial examination involved two irrigated cotton plots. In the spectral examination, good agreement was obtained between the corrected spectra and the laboratory spectra. During the spatial examination it was possible to distinguish between two cotton plots having different soil water statuses by applying the Spectra Angle Mapper (SAM) classifier. It is felt that careful selection of samples is a prerequisite for achieving reasonable results using the EL correction technique. The samples should consist of albedo information representative of the study area, should have only minor changes related to the passage of time, and should be precisely identified on both the image and the ground. It was concluded that even a 'hopeless' raw data set, such as the current GER data, can be processed to yield reasonable physical information. Assuming that future hyperspectral data taken from orbit will not often be followed by simultaneous ground measurements, the results of this paper are promising.

†email: bendor@ccsg.tau.ac.il

International Journal of Remote Sensing
ISSN 0143-1161 print/ISSN 1366-5901 online
http://www.tandf.co.uk/journals

1. Introduction

The imaging spectroscopy (IS) technique (also defined as hyperspectral remote sensing) is rapidly entering the field of remote sensing as a tool for precise and quantitative analysis of atmospheric–terrestrial systems from air. Basically it provides a near-laboratory quality spectrum of every pixel within a sensed image and allows better identification of objects based on their well-known specific absorption features (Goetz 1991). All currently available IS sensors are operational from air but new IS sensors developed for use from space are expected to provide routine global IS sensing. The GER 63-channel scanner is one of the first commercial imaging spectrometers that has proven itself over the past 10 years to be a useful tool in the fields of geology (Ben-Dor and Kruse 1995), soil science (Werner and Lehmann 1991), atmospheric science (Ben-Dor and Kruse 1996), agriculture and hydrology (Bach and Mauser 1991) and other applications. The GER sensor consists of 63 channels across the visible–near-infrared–short wave infrared (VIS–NIR–SWIR) spectral regions and uses three spectrometers, one each for the VIS (0.47–0.84 μm), SWIR-I (1.44–1.84 μm) and SWIR-II (2.00–2.45 μm) spectral regions. More information about the system can be found in Mackin and Munday (1988). All radiance information received by an onboard optical sensor is attenuated by atmospheric effects and the shape of the solar curve. If the atmospheric spectral features are not properly removed, a significant analytical bias could be introduced during the data interpretation. Removal of these effects is mandatory if remote sensing of the Earth's surface is in question. Removal of solar effects is a relatively simple task, which requires using the solar curve above the atmosphere. Whereas implementation of such information is a rather simple and straightforward process (Ben-Dor *et al.* 1994b, Ben-Dor and Kruse 1996), removal of the atmospheric attenuation is more complicated. For all practical purposes, methods that correct the atmospheric attenuation can be divided into two categories: (1) those that rely on ground data measurements taken during the flight time (both of the surface and of the atmospheric conditions) and (2) those that rely on the data themselves, where no *a priori* knowledge of the atmosphere or surface conditions is available. Methods in category 1 require field measurements to be taken during the flight time, either of the atmosphere (e.g., optical depth) or of the surface (e.g., reflectance). Atmospheric measurements are incorporated with models such as LOWTRAN-7 (Kneizys *et al.* 1988), 5S (Tanre *et al.* 1990) or Atmospheric REMoval program (ATREM) (Gao *et al.* 1993), and surface measurements are incorporated with methods such as the Empirical Line (EL) correction technique (Roberts *et al.* 1985, Kruse *et al.* 1990) or the Single Spectrum (SS) method (Crowley *et al.* 1988). Methods that use atmospheric models and measurements introduce a physical basis to the raw data correction. Methods that rely on ground reflectance measurements are based on empirical parameters and are always relative to the references used. Methods from category 2 are those that rely on entire datasets, such as the Internal Average Relative Reflectance (IARR, Kruse 1988) or the Log Residual (LR) (Green and Craig 1985) and those that use selected reference featureless pixels, such as the Flat Field (FF) method (Rast *et al.* 1991). Other methods, such as the cloud shadow technique (Carder *et al.* 1993) or the oxygen offset procedure (OOS) (Ben-Dor *et al.* 1994b), which aim to correct for aerosol scattering in the VIS region, also fall under category 2 because they use information extracted from raw data only. Kruse (1988) and Ben-Dor and Kruse (1994) discussed the limitation of methods in category 2 and stated that artefact signals may appear in the corrected dataset, depending on the area covered and on

the spatial size of the data studied. Ben-Dor *et al.* (1994a) showed that the EL method from category 1 could not effectively be applied to a raw GER dataset from Makhtesh Ramon, Israel, using only two references targets. In this regard, Ben-Dor and Kruse (1994) showed that the IARR method from category 2 is strongly biased by the spectral characteristics of all the image pixels and suggest precaution when using this correction. Artefacts are also introduced into data corrected by methods in category 1 (Farrand *et al.* 1994), however, it is possible to combine two methods, one from each category, in order to remove artefact signals (e.g., first apply ATREM and then correct with the FF method). In 1989, a GER campaign was conducted over Israel, acquiring data from four sites within the country. Because of insufficient experience at that time, regarding the IS technology in general and the collection of ground data in particular (no field spectrometers, sun photometers, etc.), no ground data was collected either during or close to the flight time. Nevertheless, for one site, Makhtesh Ramon, both Kaufmann *et al.* (1991) and Ben-Dor *et al.* (1994a) were able to correct the raw data into reflectance using methods from category 2, proving that promising analytical capabilities can be achieved from a homogeneous geological site. Except for data from the Makhtesh Ramon site, the majority of raw GER data from the 1989 campaigns have not yet been processed. This is mainly because the atmospheric correction of these ageing data seems to be hopeless for both categories, because of the lack of ground data and because of the complexity of the covered areas for categories 1 and 2, respectively.

The purpose of this paper is to examine systematically both categories to determine the availability of methods that are able today to correct raw GER data from the 1989 Israeli campaign. For that purpose we selected the most complex area then covered by the GER sensor (Naan flight line) and conducted a systematic study on how to extract reflectance information in spite of the elapsed time.

2. Areas and data used

Of the four sites covered by the 1989 Israeli GER campaign, the Naan site was selected for this study. The area is located in central Israel and is characterized by a diverse land coverage, including agricultural fields (green and dry (mostly straw) vegetation), bare soils, railroads and highways, water bodies, urban buildings, an industrial area and an open lime quarry. Figure 1 is a schematic soil map of the study area with the GER coverage overlain. The flight took place on 9 July 1989 between 11:48 and 12:00 GMT, from an altitude of 10 000 feet, which provided a pixel size of approximately 17 m. As previously mentioned, no ground data measurements were taken during or close to the time of the flight mission, although limited soil samples were collected at that time. Apparently these samples were lost in the ensuing years, so it was not possible to use them for this study. It should be pointed out that in addition to our major goal of examining possible correction techniques over this diverse landscape coverage, much of our motivation came from the desire to put 'life' into this old and 'hopeless' data in order to prove that IS data are valid at almost any time and under most conditions.

2.1. *Geometrical correction*

The raw GER data was significantly distorted along the cross-track direction. To spatially judge the results and to enable precise location of each ground sampling position, the raw image was rectified using Ben-Dor *et al.*'s (1996) steps for geocorrecting similar GER data. For that purpose, soil and road maps of the area were

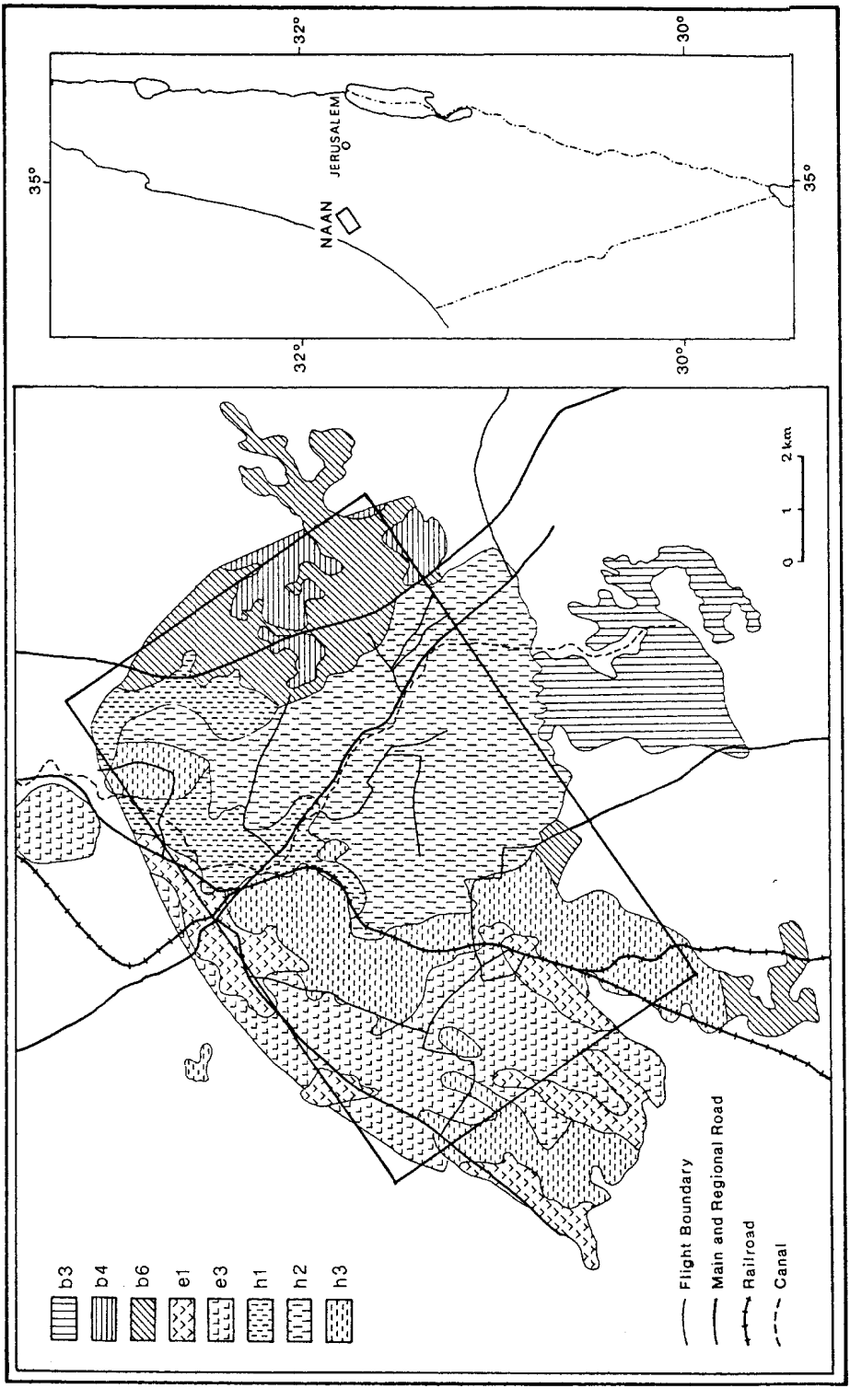

Figure 1. A soil map of the Naan area and its geographical location (see table 1 for exact definition of each soil's group).

digitized and used as a base against which the raw data were registered. To rectify the image, a map-to-image registration technique was applied using 96 ground control points (GCPs) and maintaining a rms. around 10 m (approximately half the size of a pixel). The image was warped to match the map using the Delaunay triangulation transformation technique (Devereux *et al.* 1990), where using the nearest neighbour resampling technique performed the intensity interpolation of the rectified pixels. For defining the exact sample position, the above procedure was employed on the raw digital data. For spatial examining of the results, however, the above procedures were employed only after the original data had been processed. This was done in order to avoid errors encountered while resampling the original pixels' values into new rectified artificial ones.

2.2. *Late sampling and laboratory measurements*

During the end of June 1996 (seven years after the flight), we conducted a ground sampling mission along the Naan area and collected 20 soil, rock and vegetation samples. The ground sampling was performed along sites that were assumed not to have changed over the years or assumed to have a similar seasonal composition. This included bare soils, cultivated soils (vegetation-free), rocks, green cotton leaves and dead vegetation (straw). Figure 2 presents a grey scale rectified image of the

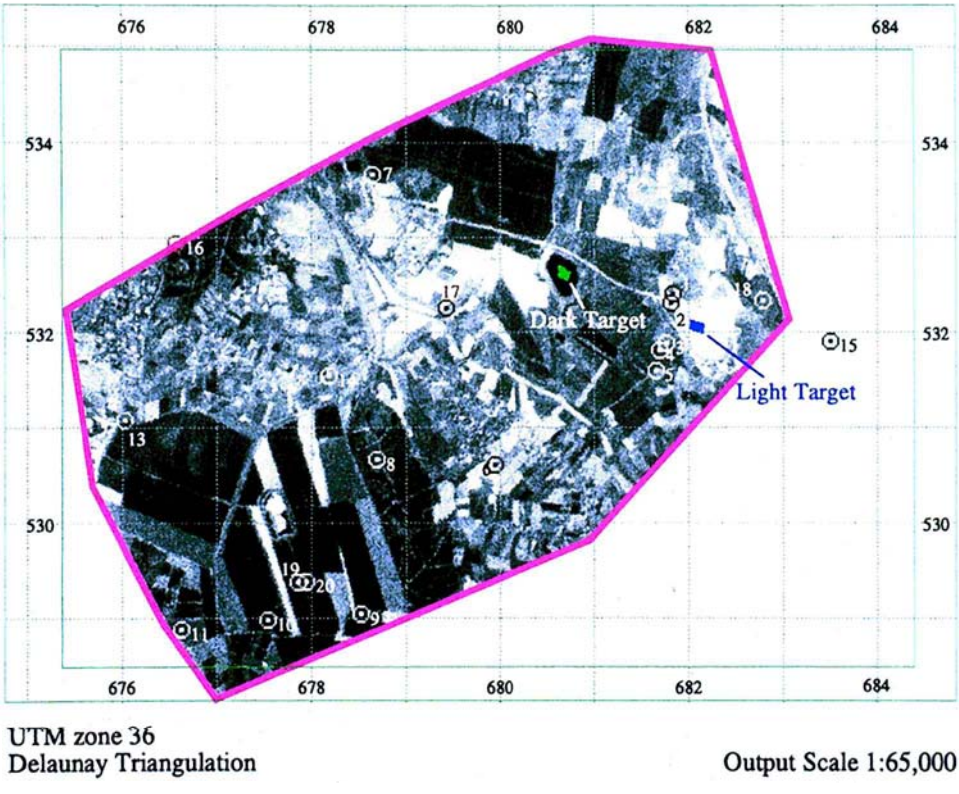

Figure 2. A grey-scale rectified image (to UTM) of the raw GER data, with the exact locations of all targets selected for this study overlain.

Naan flight line and the exact position of each sampling location. The soil samples were brought into the laboratory, air-dried for two weeks and gently crushed to allow laboratory reflectance measurements using a 10 cm diameter sample holder. In addition to the above, a cotton branch was brought into the laboratory in a water vase (to prevent water stress) and several leaves were immediately measured for their reflectance in the same spectrometer used for the soil samples. Good reproducibility of all leaves' spectra enabled the selection of one representative leaf to demonstrate the cotton vegetation. The reflectance information of each sample was recorded, using a LICOR and an LT-1200 spectrometer for the VIS–NIR (0.4–1.1 μm) and the SWIR (1200–2400 μm) spectral regions, respectively. In both spectrometers the relative reflectance spectra were calculated against Halon that was recorded under similar radiation and geometrical conditions. After the relative reflectance spectra were generated, the two spectral regions were merged and resampled into the GER 63 channel configuration. The results (termed GER-laboratory spectra) were stored in a separate spectral library for further utilization. Each of the soil samples was examined by X-ray analysis, which was performed by using unoriented powders (crushed to pass through a silt-sized sieve), a Philips diffractometer with Co Kα radiation and 2θ ranging from 3° to 40°.

3. Results and discussion

3.1. *Data quality*

3.1.1. *Signal-to-noise*

In order to judge the signal quality of the current data set, we estimated the 'signal-to-noise' ratio (SGN) according to Kaufmann *et al.* 1991:

$$\mathrm{SGN} = \mathrm{AV}/\mathrm{SD} \tag{1}$$

where AV is the signal estimated from the pixel values averaged over a homogeneous target, and SD is the noise estimated from the standard deviation of these pixel values. Figure 3 represents the corresponding SGN spectra using 64 pixels of uniform dark (a) and light (b) targets taken over a body of water and a lime quarry, respectively. From figure 3 it can be seen that the SGN values vary between 20 and

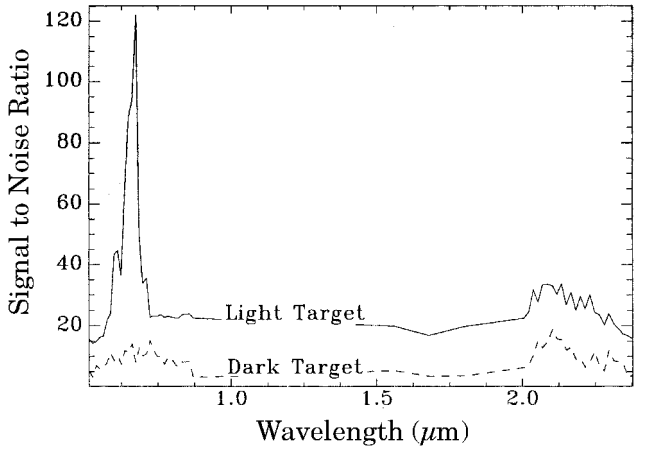

Figure 3. The signal-to-noise ratio (SGN) as derived from the light and dark targets presented in figure 2 (see text for more details).

120 in the light targets and between 1 and 15 in the dark targets. These values agree with those obtained by both Kaufmann *et al.* (1991) and Ben-Dor *et al.* (1994a) for the Makhtesh Ramon site, using a similar technique. Because data from the Naan and Makhtesh Ramon areas were acquired during the same flight, it can be concluded that, from an SGN standpoint, the GER sensor was quite stable during the 1989 Israeli campaign. It should be pointed out, however, that these SGN values still lag far behind the 5000 for the visible and near-infrared (VNIR) region and the 500 for the SWIR region that were reported by Mackin and Munday (1988) for the GER sensor.

3.1.2. *Band centring*

Two bands were omitted from the data (band 28, 0.81 μm and band 32, 1.440 μm) because of noisy spectral responses. Band centring of the SWIR spectrometer was examined on the basis of known absorption features of the carbon dioxide (CO_2) located at 2.005 μm and 2.055 μm, which were observed at 2.002 μm and 2.054 μm, respectively, in the GER radiance data. The VIS spectrometer yielded features at 0.724 μm and 0.824 μm (water vapour) and at 0.687 μm and 0.76 μm (oxygen), which were located at the expected positions for these gases. This was identical to what was observed by Ben-Dor and Kruse (1996) using the same sensor, confirming that the GER scanner was well band-centred then. However, Ben-Dor and Kruse (1996) have also noticed that the spectral response of the water vapour and oxygen at 0.687 μm and 0.761 μm, respectively, are questionable and suggested new calibration parameters for these bands. Accordingly, these new parameters were incorporated in the current dataset at the radiometric correction stage.

3.2. *Correction methods used*

As previously mentioned, we applied a 'late' EL method from category 1 using samples collected seven years after the flight. However, the first step was to apply the IARR and FF methods from category 2 and ATREM from category 1. Following are detailed descriptions of each these methods exactly as they were used in this study.

The IARR method uses a reference spectrum that is the average of all the data pixels (Kruse 1988). By dividing each raw pixel's spectrum by the reference spectrum, it is assumed that the atmospheric and solar attenuation as well as the systematic spectral noise will be removed. The IARR method does not require previous knowledge of the study area or of the data themselves (e.g., radiometric factors), and special attention must be given to the interpretation of the IARR-corrected data (Kruse 1988). The IARR's failure to effectively correct a given dataset depends on the spectral characteristics of the studied area (Kruse 1988, Mackin and Munday 1988) as well as on the spatial size of the image used (Ben-Dor and Kruse 1994). As long as the area in question consists of spectral variations that are well weighted along the scene, the IARR correction tends to produce reasonable results. However, when the area becomes more homogeneous, important surface features might disappear from the data and the corrected image may no longer reveal representative reflectance information (Ben-Dor and Kruse 1994). Another problem in the IARR method is in obtaining artificial features related to the data quality (Kruse 1988). Accordingly, in the current Naan dataset, we spatially subset the raw data and cut the noisy edges (25 pixels from both line and sample rows) before applying the IARR procedure.

The FF technique is a well-known approach from category 2 (Rast *et al.* 1991). In this method a small and spectrally uniform area (if possible a spectrally featureless area) is used as a reference target by which every pixel's spectrum is divided. In reality it is quite difficult to define an ideal (featureless) reference target, and the result may be biased by the spectral features of the selected reference. For applying the FF technique in this study, we used the same subscene used for the IARR process (edges cut) and selected the two extreme albedo targets to use for the SGN examination: dark (water) and light (open lime quarry) (see figure 2 for the exact locations). We termed these targets and the related results as FF-dark and FF-light, respectively.

Because no atmospheric information was available for the time of the flight, atmospheric-based methods from category 1 could not be directly applied. Nonetheless, using archive data taken from the closest meteorological station (Bet Dagan, about 20 km west of the centre of the image) it was possible to apply one atmospherically based method from category 1. The selected method was the ATREM 3 (modification of ATREM 1, Gao *et al.* 1993), which relies on very general atmospheric information. The ATREM (ATmospheric REMoval) program was originally developed to correct AVIRIS data into 'scaled surface reflectance' over flat terrain areas. The Malkmus narrow band model and a pressure scaling approximation are used in calculating atmospheric transmittances of all gases. The atmospheric scattering is modelled by using a 5S code, and the column water vapour is estimated by using the relative water absorption at around 0.94 μm and 1.14 μm. The program uses six general atmospheric models and four aerosol models (taken from LOWTRAN-7) to best describe the conditions (except for the geographic location, the area elevation and the date of the flight) during the overflight. The only 'ground data' information required by the program is the visibility (or if available, the optical depth) at the time of the flight. Accordingly, we ran ATREM 3 with the following parameters: wavelength and full width half maximum (FWHM) of the GER scanner, all gases selected with a total column ozone of 0.34, atmospheric models of mid-latitude summer, continental aerosol model and a visibility of 100 km.

Another selected method from category 1 was the EL correction technique that relies on ground spectral information (Roberts *et al.* 1985). In general, the EL method uses a linear fit between field (or laboratory) and raw spectral data of high and low albedo targets, which applies to every wavelength. The parameters (gain and offset) of this linear fit are then applied to the raw data on a pixel-by-pixel basis to yield a new EL-corrected cube. The EL technique has been widely and successfully used by many IS workers (e.g., Kruse *et al.* 1990, Farrand *et al.* 1994). Because a given EL process may yield poor results if the reflectance of the selected sample does not accurately represent the pixels selected from the image and because a late sampling was performed, we took the following four precautions: (1) We selected targets that were assumed not to have been changed over the years (soil, rocks and seasonal vegetation). (2) We did not aggressively crush the samples for the reflectance measurements (in order to preserve the field condition as much as possible and maintain the grain size within a reasonable orientation for the sensor's field of view). (3) We selected areas that showed a uniform spatial distribution. (4) We geolocated the targets as precisely as possible both on the image and on the ground. Based on Ben-Dor *et al.*'s (1994a) poor results using the EL approach with two samples for the Makhtesh Ramon dataset, we ran the EL method using three different combination stages as follows:

Stage a: a stage consisting of two samples representing extreme lambertian (soil) albedo behaviour of the scene: light and dark targets (sample no. 2 and sample no. 6 (in table 1), respectively, designated as EL-light, 6).

Stage b: a stage consisting of three samples representing albedo variation sequence over the scene (as emerged from the baseline height of each target's radiance spectrum): light, intermediate and dark targets (sample no. 2, sample no. 18 and sample no. 5 (in table 1), respectively, designated as EL-light, 5, 18).

Stage c: a stage consisting of five samples representing the spectral variation along the scene (as emerged from the spectral features of each target's radiance spectrum) (sample no. 2, sample no. 20, sample no. 19, sample no. 6 and sample no. 18 (in table 1) designated as EL-light, cotton, straw, 6, 18).

The laboratory spectra (GER-laboratory) of all the samples used in the EL stage are given in figure 4. Table 1 shows the basic mineralogy of each sample and its soil classification name, according to the United States Department of Agriculture (USDA) and local Israeli classification systems. Six soil groups exist in the area, and all groups are represented by the selected samples. As can be extracted from the X-ray analyses (see table 1), each of the examined soils consisted of quartz, calcite and montmorillonite in various proportions, with impurities such as iron oxides and other clay minerals introduced.

3.3. *Data correction*

In order to assess each method's capability for correcting for atmospheric attenuation, independent samples (not included in the correction procedures) were used. In figure 5 the GER-laboratory spectra (A) of validation targets with their corresponding GER-corrected (IARR (B) FF-light (C) and FF-dark (D)) spectra are given to represent results from category 2.

In this stage, the validation samples were selected to represent all soil groups of the area (see table 1). As can clearly be seen from figure 5, none of the IARR or FF methods provided a good or even reasonable spectral match between the GER-

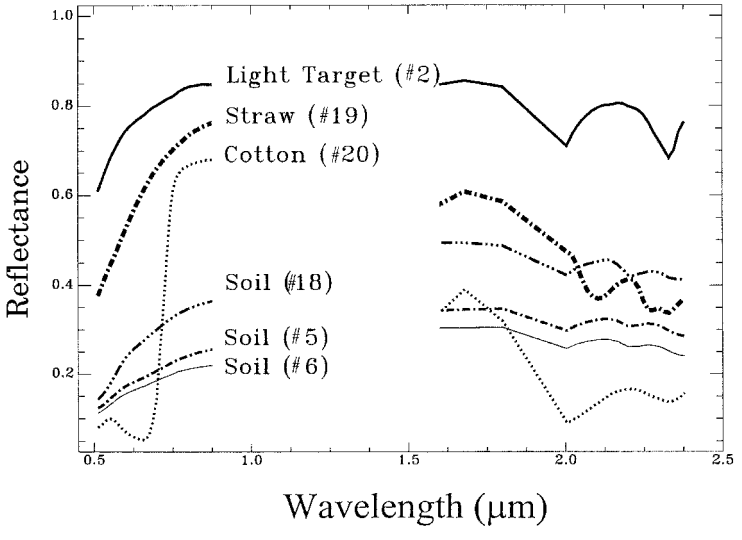

Figure 4. The laboratory spectra (resampled into the 63 GER channels) of six samples used to run the EL-correction technique.

Table 1. General information (soil groups and basic mineralogy) of the targets selected for this study. The exact position of each sample is given in figure 2.

Code	Description	Israel and USDA soil classification	Mineral composition
Sample 1	lime quarry (side)	not a soil	clacite+ + + + +, dolomite+, quartz+, illite+
Sample 2	lime quarry (centre)	not a soil	calcite+ + + + +, dolomite+, quartz+
Sample 3	bare field	brown–red–grumosols (h2), xerert	quartz+ + + +, montmorillonite+ +, kaolinite+, calcite+
Sample 4	soil of agricultural field (wild vine)	brown–red–grumosols (h2), xerert	quartz+ + +, montmorillonite+ + + +, kaolinite+, quartz+ +
Sample 5	soil of agricultural field (wheat)	brown–red–grumosols (h2), xerert	quartz+ + +, calcite+ + +, montmorillonite+ +, kaolinite+, iron oxides+
Sample 6	soil of agricultural field (oranges)	brown–red–grumosols (h2), xerert	quartz+ + + +, calcite+ + +, montmorillonite+ +, kaolinite+
Sample 7	soil of agricultural field	brown–alluvial–grumosols (h1), xerert	quartz+ + + + +, calcite+ + + +, montmorillonite+, kaolinite+
Sample 8	soil of agriculture field	brown–red–grumosols (h2), xerert	quartz+ + + +, calcite+, montmorillonite+
Sample 9	soil of agricultural field	brown–red–grumosols (h2), xerert	quartz+ + + +, calcite+, montmorillonite+
Sample 10	soil of agricultural field (cotton)	brown–accumulative–grumosols (h3) xerert	quartz+ + + + +, montmorillonite+, illite+, kaolinite+
Sample 11	bare field	hamra (e3), rhodoxeralf	quartz+ + + +, montmorillonite+, iron oxides+
Sample 12	bare field	brown–red–grumosols (h2), xerert	quartz+ + + +, montmorillonite+ + +, illite+, kaolinite+, calcite+
Sample 13	bare field	brown–red–grumosols (h2), xerert	quartz+ + + +, montmorillonite+ + +, kaolinite+, calcite+
Sample 14	agricultural field	brown–red–grumosols (h2), xerert	quartz+ + + + +, calcite+ + +, montmorillonite+ +, illite+, kaolinite+
Sample 15	bare field	dark–brown–rendzina (b6), haploxeroll	quartz+ + +, calcite+ +, montmorillonite+ +, illite+
Sample 16	bare field	hamra with gley (e1), rhodoxeralf	quartz+ + + + +, montmorillonite+, iron oxides+
Sample 17	bare field	brown–alluvial–grumosols (h1), xerert	quartz+ + +, calcite+ +, montmorillonite+ +, kaolinite+
Sample 18	bare field	brown–rendzina (b4), haploxeroll	quartz+ + +, calcite+ +, montmorillonite+ +, kaolinite+, iron oxides+
Sample 19	straw	not a soil	
Sample 20	cotton leaf	not a soil	

+ + + + + hi; + + + + hi-moderate; + + + moderate; + + moderate-low; + low.

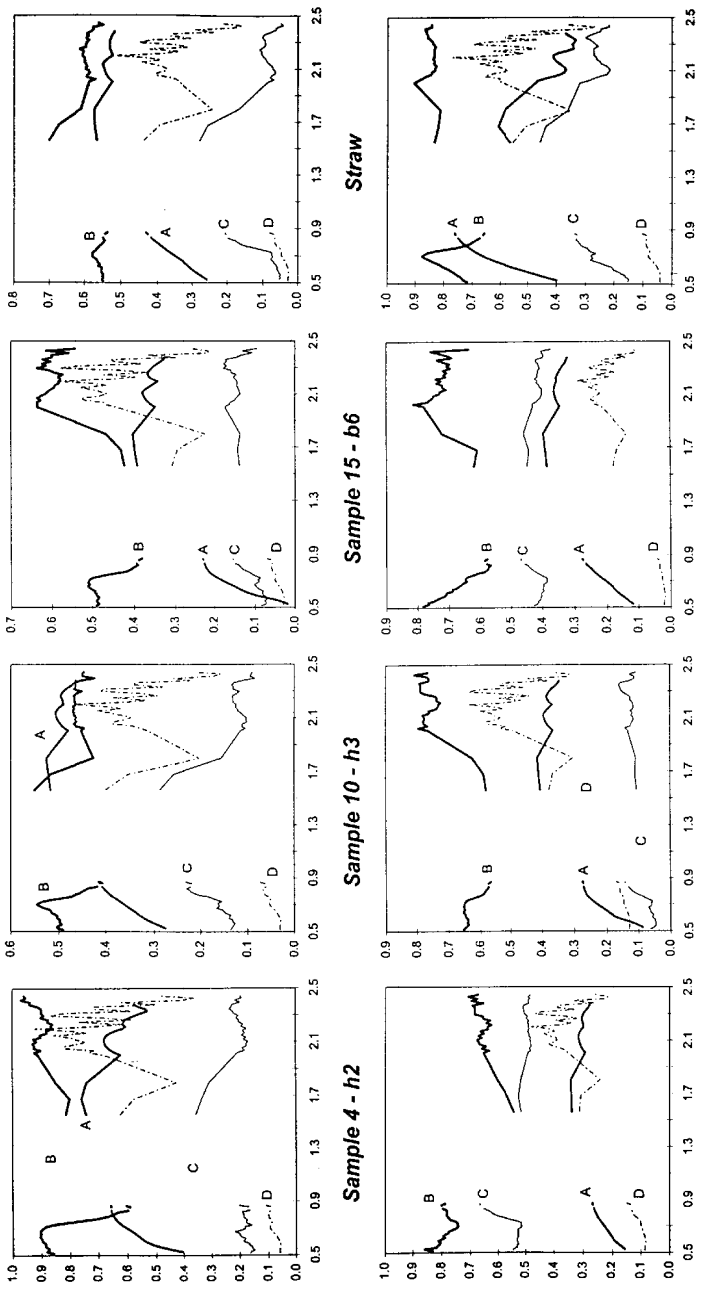

Figure 5. Validation spectra of the FF correction, in both the (C) light (FF-light) and (D) dark (FF-dark) targets and (B) the IARR correction compared with (A) a corresponding laboratory spectrum resampled into the 63 GER channels (LAB).

laboratory and the GER-corrected spectra. The conclusion to be drawn from this stage is that neither the IARR nor the FF (light or dark) techniques can, under the given conditions, correct the current raw GER data into apparent reflectance. The FF failure is probably because of the fact that the reference targets were not suitable for that purpose. The FF-light target (limestone) was not featureless, and the FF-dark target (water body) had low spectral signals and high noise across most of the spectral region. Apparently no appropriate light target, such as a sand dune, existed within the area, and, therefore, the correction was inadequate. The failure of the IARR method to correct the data is probably because of the extreme complexity of the landscape from both an albedo and a spectral standpoint. It is interesting to note, however, that along the Makhtesh Ramon flight line (taken one hour prior, using the same sensor), both the FF and IARR methods revealed very reasonable results (Kaufmann *et al.* 1991, Ben-Dor *et al.* 1994a). As already discussed, the Naan and Makhtesh Ramon data sets were found to have similar spectral and SGN responses. For this reason, it is assumed that the disagreement between the IARR and FF results in the two sites can more likely be attributed to the landscape differences. Whereas in the Makhtesh Ramon area, vegetation is scarce and the mineralogy distribution along the scene is diverse and well spread, in the Naan area, the surface is covered by dense vegetation (green and dry) and by a complex mixture of water bodies, roads, suburban areas, a quarry and so forth, which are not equally distributed along the scene.

At this point, we applied the ATREM program in order to see whether an atmospherically based method from category 1 could improve the results. In figure 6 the ATREM-corrected spectra (E) of the same targets used to examine category 2 (figure 5) are presented along with other corresponding results (EL-corrected spectra; see later discussion). As clearly seen in figure 6, ATREM-corrected spectra (E) revealed poor with the laboratory spectra of all samples (A). Basically, the ATREM program calculates the amount of water vapour on a pixel-by-pixel basis based on two water vapour bands in the NIR spectral region (for the current dataset we used 0.687 μm and 0.724 μm). The derived water vapour values are then used for water vapour absorption effects in the entire 0.4–2.5 μm region. As can be clearly seen, the ATREM failed to correct the atmospheric features at all water vapour absorption peaks (at 0.687 μm, 0.724 μm and 1.8 mm). We suspect that this failure is due to incorrect calibration of radiometric values of the basic features used to estimate the water vapour content at 0.687 μm and 0.724 μm. Referring to Ben-Dor and Kruse's (1996) encounter with radiometric problems in two bands (no. 18, 0.687 μm and 0. 24, 0.761 μm), these results may indicate that the entire spectral region between 0.678 μm and 0.83 μm was radiometrically miscalibrated.

In spite of the poor correction of the water vapour features, ATREM reasonably corrected other attenuation across the VIS spectral region (0.477–0.662 μm). This can be seen from the good match achieved between the ATREM-corrected spectra and the laboratory spectra of the validation targets. In this region the ozone absorption and atmospheric scattering fully removed. Across the SWIR region (2.005–2.443 μm), however, spectral artefacts clearly emerged after ATREM was applied. In reality, these artefacts are the major problem of the ATREM program even with well-calibrated IS data (Boardman and Huntington 1997). It therefore can be concluded that the ATREM program has not provided a confidence limit for correcting the atmospheric attenuation for the current data set. More generally it can also be concluded that atmospheric-based models may introduce two basic

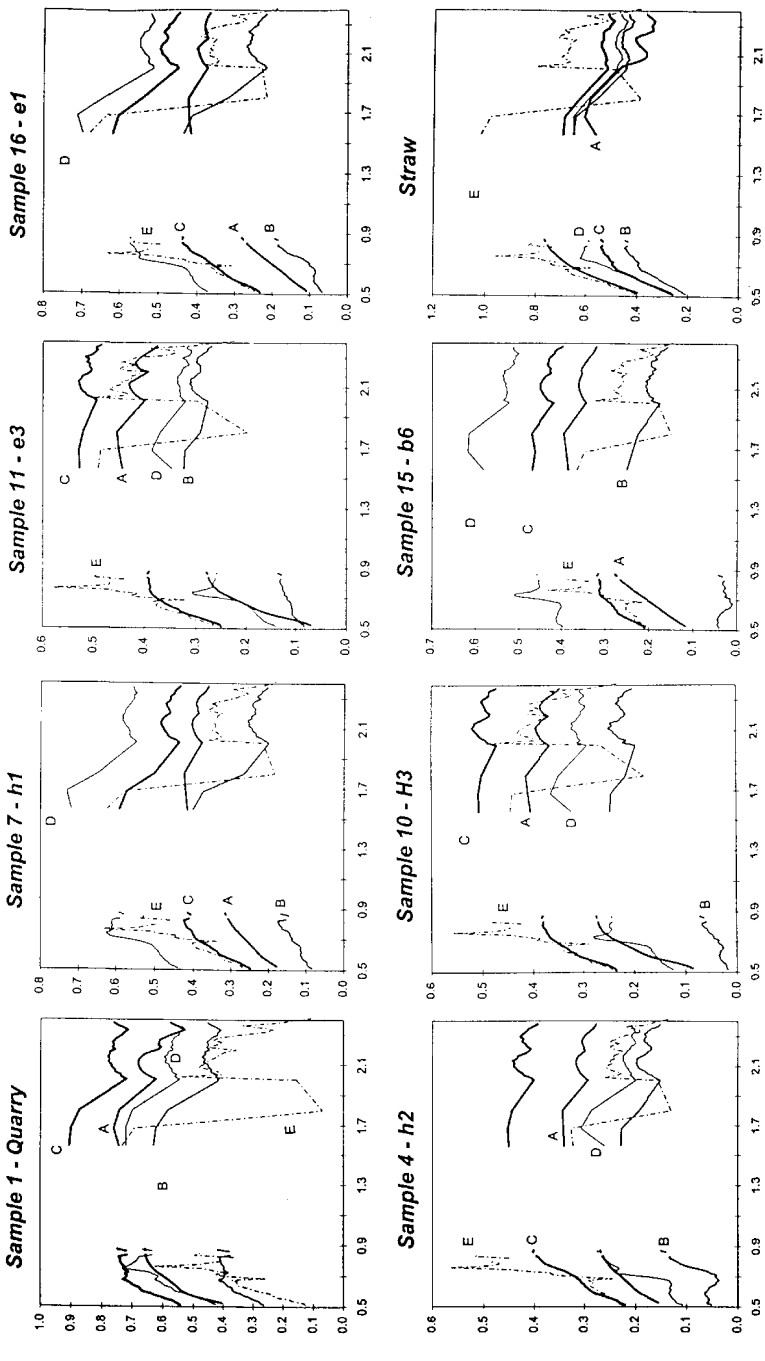

Figure 6. Validation spectra of the EL correction results for the three combinations used: (B) EL-light, 6 (samples nos 2 and 6 in table 1, respectively) for stage a; (C) EL-light, 5, 18 for stage b (samples nos 2, 5 and 18 in table 1, respectively); (D) EL-light, cotton, straw, 6, 18 for stage c (samples nos 2, 20, 19, 6 and 18 in table 1, respectively). Also provided are the ATREM correction results of these targets (E). A comparison is made between each spectrum and its corresponding laboratory spectrum (A), resampled into the 63 GER channels (LAB).

problems when they are applied over elapsed time: (1) no exact information is available in order to precisely model the atmospheric conditions; and (2) there is no possibility investigate the exact radiometric sensor response. In the current ATREM program, significant (unexplained) artefacts across the SWIR region may be another major problem preventing a precise atmospheric correction.

The next step was to apply the EL method from category 1, which was the only method remaining for correcting the data. For that purpose we applied the three stages a to c previously described. Figure 6 presents the results of the EL analysis using the same samples that were used for the IARR, FF and ATREM validations. As can clearly be seen, a perfect spectral feature match was obtained between the GER-laboratory spectra (A) and the GER-corrected (EL) spectra of all samples, using stage b of the EL correction technique ((C)—EL-light, 5, 18). This combination consists of three targets having a good albedo sequence (see figure 2). To examine further this match, another five validation samples, representing two soil groups from the area, were examined. In figure 7 the GER-laboratory and GER-corrected (EL) spectra of these samples are shown. Again, very good agreement was obtained between the laboratory and corrected spectra across the entire VIS–SWIR regions,

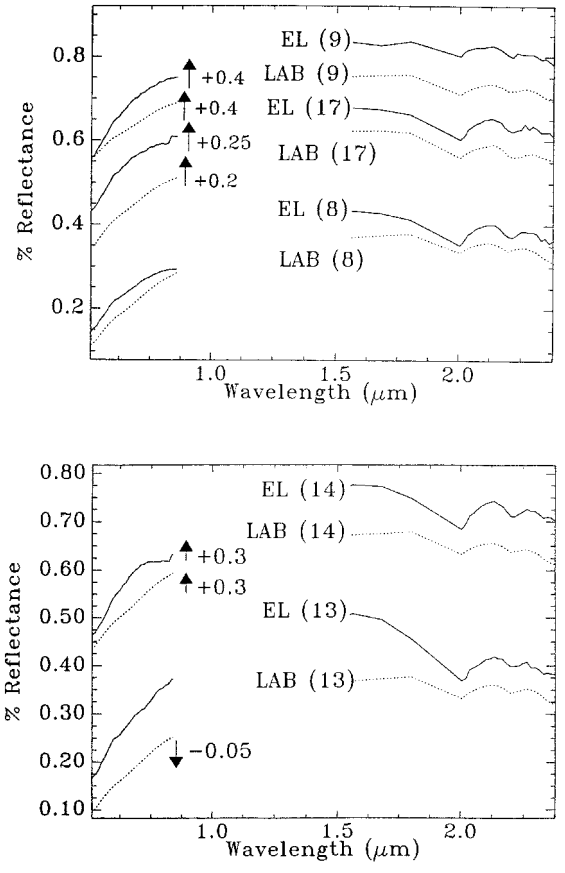

Figure 7. Validation spectra of additional soil samples not included in the correlation procedure (the sample numbers from table 1 are in brackets) using stage b of the EL correction technique (the arrows present offset used for clarity).

which adds additional support to the conclusion that the EL stage b technique is the best of all those examined. Taking into account the poor operating conditions available for correcting the current raw data, the results obtained using stage b prove to be very promising.

In order to emphasize and illustrate step-by-step the selected correction method (EL, stage b), we used three additional samples and presented them as raw, radiance, solar removal, GER-corrected (EL) and GER-laboratory spectra (LAB). The targets were limestone (sample no. 2), cotton vegetation (sample no. 20) and soil (sample no. 7). Figure 8 shows the above-mentioned spectra in the order described. It can be clearly seen that each stage provides additional spectral information. Whereas the raw digital number (DN) data in figure 8(*a*) provide no physical information, the radiance data in figure 8(*b*) show very clearly the solar effect (maximum around 0.52 μm) and the atmospheric attenuation of gases (significant peaks across the

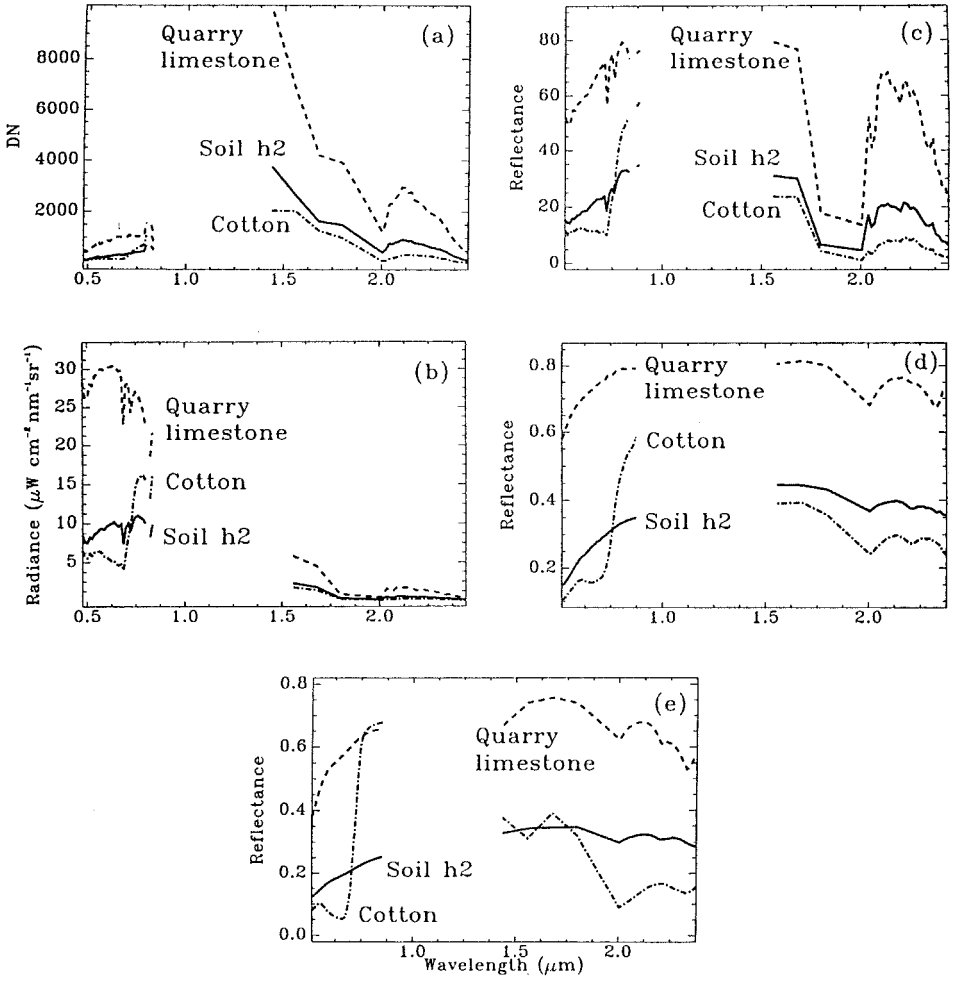

Figure 8. A series of spectra showing changes in three samples from one treatment to another (quarry limestone, sample no. 2; soil, sample no. 7; and cotton, sample no. 20). (*a*) Raw (DN) data, (*b*) raw (radiance) data, (*c*) transmittance/reflectance data, (*d*) EL (stage b)-corrected data, (*e*) laboratory data (resampled to the GER channel configuration).

spectrum). In the solar removal spectra in figure 8 (*c*) the surface and gas features become more enhanced where no solar effect is observed. In the EL-corrected spectra in figure 8(*d*) no evidence for atmospheric gases is introduced, and the spectral features obtained all represent well-known surface features. Comparing the EL-corrected spectra in figure 8(*d*) to their corresponding laboratory spectra in figure 8(*e*) again shows a perfect match between the two sets. However, careful observation revealed that an inconsistency appears at around 2.2 μm in the cotton spectra. Whereas in the GER-corrected spectrum this spectral feature is relatively significant, in the GER-laboratory spectrum it is absent. The GER-laboratory spectrum was taken from a single cotton leaf, and the GER-corrected spectrum was derived from the average of 24 pixels across the cotton field. At this time of the year (beginning of July), the cotton plants were not covering the entire surface area, and the resulting GER spectrum is a spectral mixture of both soil and vegetation. The 2.2 μm feature in the GER-corrected spectrum corresponds to the lattice OH absorption feature (a combination mode of the $\upsilon_{OH} + \delta_{OH}$ fundamentals) of the montmorillonite mineral, which is the major clay mineral in the local Israeli soils (Banin and Amiel 1970; see also the X-ray results). These results, combined with the previous validation examination, strongly suggest that the selected EL technique is very reasonable and that the corrected data has meaningful spectral information.

A major conclusion to be drawn from this section is that a 'late' EL correction procedure is possible. For this purpose, however, it is important to run more than one traditional sample combination (light and dark targets). This is mainly because with such an empirical approach, it is essential to apply several runs until the best combination emerges. The best combination is believed to combine and cover both spectral and spatial information along the study scene. It is therefore assumed that the following are the key factors needed to provide reasonable results in a 'late' EL correction: (1) knowledge of precise geolocation of the reference targets, (2) selection of targets having minor temporal variations, (3) selection of good targets in terms of albedo variation, (4) selection of targets having the major soil types of the area studied, and (5) use of 'unharmed' soil samples. Because it is sometimes impossible to achieve all of these conditions in one sample combination, several combinations must be run until reasonable results are achieved.

3.4. *Quantitative spatial analysis based on the derived spectral information*

3.4.1. *Quantitative analysis of vegetation*

In order to spatially validate the corrected data, we ran a spectrally based classification using the corrected apparent reflectance information from stage b of the EL correction technique. The analytical method was selected to provide more information on the vegetation status, in addition to studying the area during the flight time. To roughly locate the vegetation pixels, a traditional NDVI image was generated using the 0.786 μm and 0.588 μm wavelengths as NIR and VIS channels, respectively. In figure 9(*b*), the rectified NDVI image is given, and it shows that areas can be categorized according to high and low vegetation coverage. During the summertime the entire area is rather dry. High NDVI values represent areas with intensive agricultural activity and water irrigation. Likewise, low NDVI values represent bare areas, having coverage of either very little green vegetation or bare soils with dry vegetation (mainly straw). For studying the spatial information of the GER-corrected data with respect to the vegetation status, the Spectra Angle Mapper (SAM) classifier was applied (Boardman 1991). Basically, SAM determines the

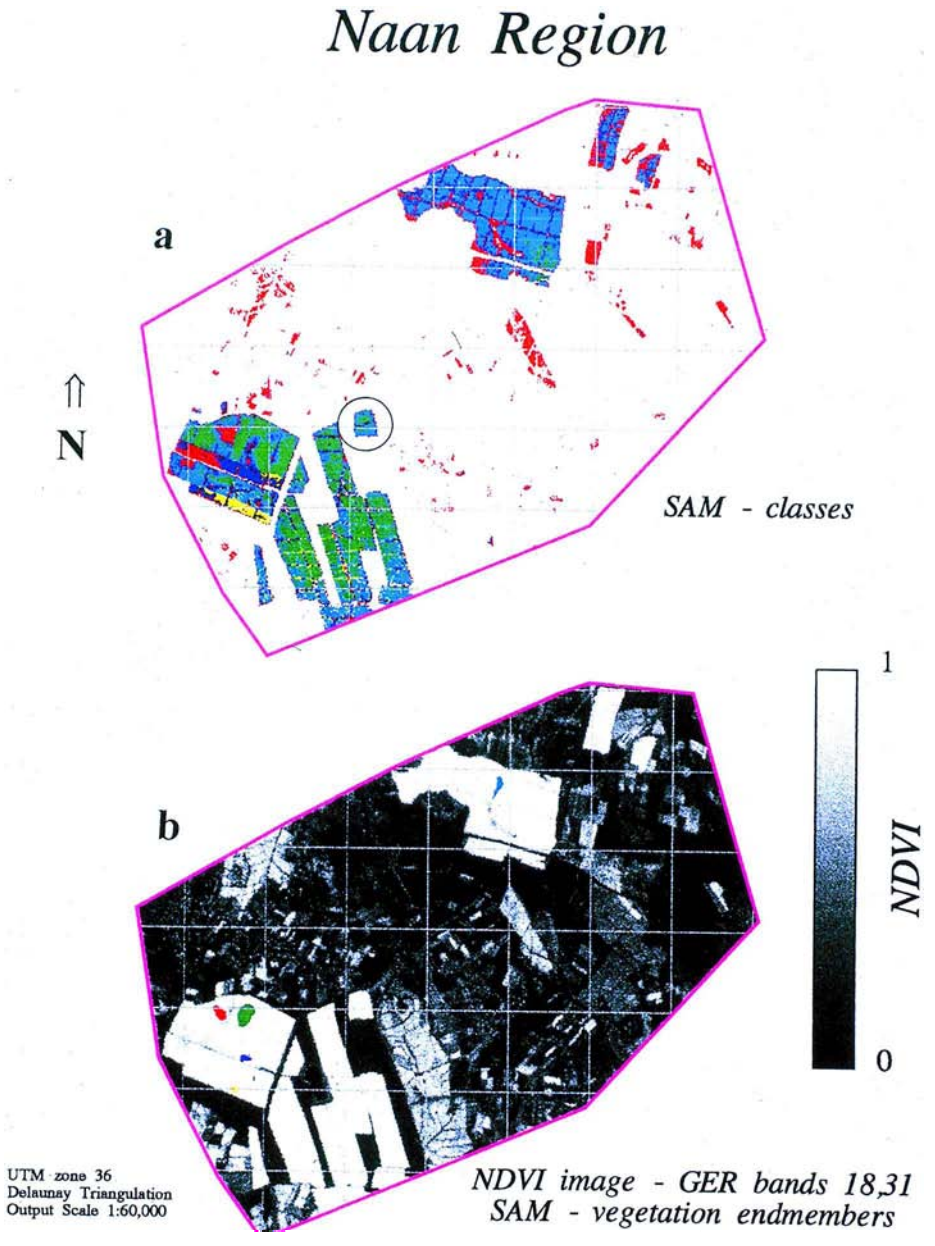

Figure 9. The rectified SAM classification image (*a*) and rectified NDVI image of the study area (*b*). Endmember positions are given on the NDVI image, and the class colour refers to each endmember. The circled plots on image (*a*) refer to irrigated (green) and nonirrigated (blue) cotton fields, as discussed in the text.

spectral similarity of selected spectra by calculating the angular difference between two spectra, treated as vectors in nb space (nb = number of bands). Although the procedure yields a view of the spatial distribution of the selected endmembers, the

more accurate the spectral information is the better the classification accuracy obtained. Thus, we used a continuous spectrum from 0.43 μm to 2.33 μm (with no 'bad' bands) in order to include the spectral information between all GER spectrometers.

Representative endmembers (EM) from the vegetated areas were selected using the NDVI image and n-dimension visualizer using all spectral bands. Doing so revealed five significant endmembers, whose spectra are given in figure 10. Their exact locations are overlain (in colour) on the NDVI image (figure 9(*b*)). A threshold (maximum) angle of 0.1 rad was used in order to generate a SAM classification image of each endmember. From figure 10, which presents the GER spectra of the five selected endmembers, it is postulated that significant spectral differences can be obtained among the endmembers. Around the chlorophyll-associated peak at 0.68 μm, a significant peak enhancement going from EM-5 to EM-1 is visible. A careful observation of this region also reveals a slight red edge shift going from EM-1 (0.662 μm) via EM-4 (0.675 μm) to EM-5 (0.699 μm). Likewise, a significant increase in the spectra slope at the near-infrared shoulder can be seen for all endmembers as well as sequence changes of the absolute length of this shoulder.

In the SWIR-I region, some spectral differences can also be observed: In EM-1, the SWIR-I slope between 1.56 μm and 0.848 μm is significantly stronger than it is in EM-5. The intermediate endmembers (EM-2, EM-3 and EM-4) also have slope differences across this region, which lies between the slope values represented by EM-5 and EM-1. This slope is mainly affected by the near-infrared shoulder just discussed and by the magnitude of the slope between 1.68 μm and 1.56 μm. We speculate that the latter is an indicator of the liquid water content located at around 1.45 μm. As more water content is available, the 1.68 μm/1.56 μm slope increases. This of course makes the 1.56 μm/0.848 μm line steeper, presumably giving an indication of the status of the vegetation's health.

Although traditionally the SWIR-II region does not provide much information

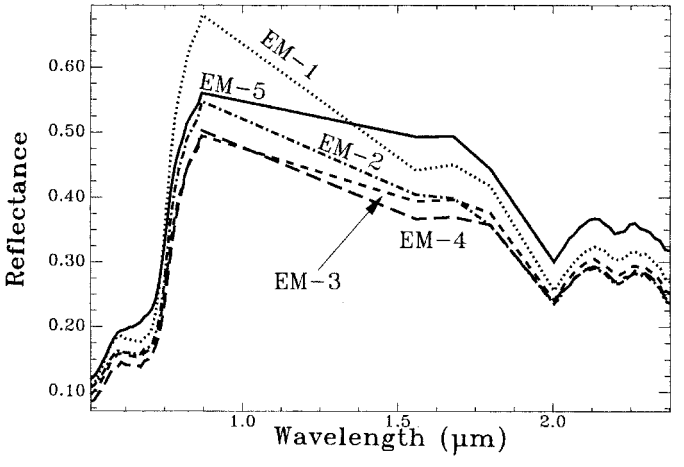

Figure 10. The spectra of the five endmembers selected for the SAM analysis, as extracted from the GER-corrected (EL, stage b) data. The exact position of each Region Of Interest (ROI) used to produce these spectra is given in figure 9(*b*). EM-5 refers to red pixels, EM-4 to yellow pixels, EM-3 to blue pixels, EM-2 to cyan pixels and EM-1 to green pixels.

about vegetation, a careful examination of this region shows a correlation with other spectral findings. Whereas in all endmembers, the 2.20 μm peak is clearly pronounced because of the soil–vegetation mixture, in EM-5, this peak (and others shown in this region) consists of a slight, but noticeable 'tooth sour' presentation. Ben-Dor *et al.* (1997) pointed out that fresh organic matter in this region shows features of organic components (C= C, C– H of starch, lignin and wax). Gao and Goetz (1994) showed that such features can be mimicked if liquid water is removed from the vegetation's structure. We therefore make a strong assumption that the low amount of liquid water in EM-5 enhanced the organic features and produced a 'noisy' SWIR spectrum. A variation among the albedo values of all endmembers is also noticeable in the SWIR region. Whereas the spectral differences among EM-1, EM-3 and EM-5 are striking, careful observation of the intermediate endmembers (EM-2, EM-3 and EM-4) also reveals significant spectral variation as was previously discussed. Thus, it can be assumed that the five selected endmembers more likely represent a possible vegetation sequence ranging from a 'healthy' (EM-1) to a 'stressed' (EM-5) condition. It should be pointed out that all endmembers' pixels were significantly segregated by the n band visualizer, suggesting favourable selection of these endmembers for classification purposes.

Figure 9(*a*) provides a rectified SAM classification image based on the five chosen endmembers. This image shows the spatial variation of the condition of the vegetation along the scene. Two main areas are visible in figure 9(*b*), located at the north-east side and at the south-west side of the image. These areas are all cotton fields and consist of relatively high NDVI values (figure 9(*b*)). It is interesting to note, however, that outside these plots, some pixels (red) were classified as EM-5 ('stressed' vegetation). At this time of the year (beginning of July), vegetation in nonagricultural fields is relatively dry and obviously is very stressed in terms of water availability. It is interesting to note that similar 'stressed' pixels are located along the cotton field itself. This suggests that even within irrigated plots, some local problems occur regarding vegetation/water status.

3.4.2. *Spatial validation*

Although this observation cannot be validated against available information on a large scale, in one case, it was possible to locally validate the assumption. Information gathered either from farmers or from an annotated air photo taken close to the time of the flight campaigns enabled the location of two close cotton plots that were irrigated differently for the GER mission (circled plot on the southern area). As can clearly be seen from the SAM image, one plot is associated with EM-1 (green) and the other with EM-2 (cyan) endmembers. As previously discussed, EM-1 represents healthy vegetation. EM-2 represents the next, less-healthy stage, which suggests a stress sequence. The pixels of the two endmembers match closely with the irrigated (green) and nonirrigated (cyan) plots, showing from this viewpoint that the atmospheric correction and the endmember selection were more than reasonable. Although we have no information regarding the status of other endmember plots during the time of the flight, based on the good results obtained by both the spectral and the spatial validation checks, we can safely assume that the SAM classification provides a reasonable picture of vegetation-stress status in the examined area.

Although such steps might be examined using additional data sets, the current case study strongly demonstrates that such a correction is feasible. This conclusion may be very useful in the IS field: (1) it might enable correction of old so-called

'useless' data, (2) it can be used as a tool for condensing soil samples long after flight times, and (3) it might serve as a tool for correcting data taken from orbit. This last is doubly important with regard to the forthcoming IS satellites because it will enable atmospheric correction of data gathered over many of the Earth's areas that are not simultaneously covered on the ground, and it may serve as a tool for correcting possible radiometric drifts of the onboard detector device.

4. Summary and conclusions

It was shown that a reasonable atmospheric correction can be made to raw IS data, even if no ground data was acquired at the flight time. Furthermore, it was shown that 'late' ground sampling is feasible for correcting the data, using methods from category 1 (designated as methods that rely on ground data measurements). The ground sampling should be performed using areas that have seen only minor variations over time and along pixels that are clearly identified on both the image and on the ground. It was suggested that if no ground data is available, first methods from category 2 should be run (e.g., IARR and FF) followed if possible by a method that relies on general atmospheric information from category 1 (e.g., ATREM). Only then should methods from category 1 that rely on ground sampling and measurements (e.g., EL) be applied. More than one configuration of the EL method on a trial-and-error basis should be applied in order to obtain reasonable reflectance results. Validation examinations must be performed against samples that were not involved in the correction procedure, and every spectrum should be carefully inspected. In this study it was found that of the four methods examined (ATREM, IARR, FF and EL), the EL with a certain configuration yielded the best results. We believe that the best EL correction was obtained because of good albedo representation of the image, accurate ground identification of the samples used for the correction and the occurrence of only minor changes of the targets' composition over time. Based on the good spectral quality obtained using the selected EL technique and on the careful validation examination performed, a SAM analysis was applied in order to examine the condition of the vegetation. The results showed that a spatial health/stress sequence of the vegetation's condition can be extracted. In one case, it was possible to validate the SAM classification results against water availability in two close cotton plots. In the near future, when IS systems are placed in orbit, ground data will not be always be available for all places on the globe and possible radiometric drift may occur over time. This methodology may be helpful to overcome such obstacles. In addition, the results of this study indicate that even so-called useless IS data may yield reasonable spectral information.

Acknowledgments

The authors want to express their gratitude to Professor A. Singer and Mrs Z. Hochman from the Soil and Water Department, Faculty of Agriculture, Hebrew University of Jerusalem for the X-ray analyses. Also our gratitude to Dr A. Karniely, Blauebstein Institute for Desert Studies, for providing the LICOR spectrometer. Special thanks go to Professor J. Otterman from NASA Goddard Space Center for reading the manuscript and for providing useful comments. Many thanks also go to Mrs K. Heidelbrecht from CSES, CIRES University of Colorado at Boulder for modifying the ATREM 3 program to work under the GER configuration. This study was supported by the Israeli Science Foundation.

References

BACH, H., and MAUSER, W., 1991, The application of imaging spectroscopy data in agriculture and hydrology. The EISAC-98 Campaign in the Freiburg test site. *EARSeL Advances in Remote Sensing*, **1**, 34–42.

BANIN, A., and AMIEL, A., 1970, A correlation study of the chemical and physical properties of a group of natural soils of Israel. *Geoderma*, **3**, 185–198.

BEN-DOR, E., and KRUSE, F. H., 1994, The relationship between the size of spatial subsets of GER 63 channel scanner data and the quality of the Internal Average Relative Reflectance (IARR) atmospheric correction technique. *International Journal of Remote Sensing*, **15**, 683–690.

BEN-DOR, E., and KRUSE, F. A., 1995, Surface mineral mapping of Makhtesh Ramon, Negev, Israel using GER 63 channel scanner data. *International Journal of Remote Sensing*, **16**, 3529–3553.

BEN-DOR, E., and KRUSE, F. A., 1996, Detection of atmospheric gases using GER 63 channel scanner data acquired over Makhtesh Ramon, Negev, Israel. *International Journal of Remote Sensing*, **17**, 1215–1232.

BEN-DOR, E., KRUSE, F. H., LEFFKOFF, A. B., and BANIN, A., 1994a, Comparison of three calibration techniques for utilization of GER 63-channel aircraft scanner data of Makhtesh Ramon, Negev Israel. *Photogrammetric Engineering and Remote Sensing*, **60**, 1339–1354.

BEN-DOR E., GOETZ, A. F. H., and SHAPIRO, A. T., 1994b, Estimation of cirrus cloud and aerosol scattering in hyperspctral image data. *Proceedings of the International Symposium on Spectral Sensing Research II:, ISSSR San Diego, California*, pp. 582–593.

BEN-DOR, E., KRUSE, F. A., DIETZ, J. B., BRAUN, A. W., and BANIN, A., 1996, Spatial distortion and quantitative geological mapping of Makhtesh Ramon, Negev Israel by using the GER 63 channel scanner data. *Canadian Journal of Remote Sensing*, **22**, 258–268.

BEN-DOR, E., INBAR, Y., and CHEN, Y., 1997, The reflectance spectra of organic matter in the visible near-infrared and short wave infrared region (400–2500 nm) during a controlled decomposition process. *Remote Sensing of Environment*, **61**, 1–15.

BOARDMAN, J. W., 1991, Sedimentary facies analysis using imaging spectrometry: a geophysical inverse problem. PhD dissertation, University of Colorado, USA.

BOARDMAN, J. W., and HUNTINGTON, J. F., 1997, Mineralogic and geochemical mapping at Virgina City, Nevada, using 1995 AVIRIS data. *Proceedings of the Twelfth International Conference and Workshop on Applied Geologic Remote Sensing, Denver, Colorado, 17–19 November*, I-191–198.

CARDER, K. L., REINERSMAN, P., and CHEN, R. F., 1993, AVIRIS calibration using the cloud-shadow method, *Summaries of the Fourth Annual JPL Airborne Geoscience Workshop, AVIRIS Workshop, JPL Publication* 93-26, Pasadena, California, edited by R. O. Green, pp. I:15–18.

CROWLEY, J., ROWAN, K., and PODWYSOCKI, M., 1988 Evaluation of airborne Visible/Infrared Imaging Spectrometer (AVIRIS) data of the Mountain Pass, California carbonate complex. *Proceedings of the Airborne Visible/Infrared Imaging Spectrometer (AVIRIS) Performance Evaluation Workshop, JPL Publication* 88-38, Pasadena, California, pp. 155–161.

DEVEREUX, R. M., FULLER, R. M., CARTER, L., and PAESELL, R. J., 1990, Geometric correction of airborne scanner imagery by matching Delaunay triangles. *International Journal of Remote Sensing*, **12**, 2237–2251.

FARRAND, W. H., SINGER, R. B., and MERENYI, E., 1994, Retrieval of apparent surface from AVIRIS data: a comparison of Empirical Line, radiative transfer and spectral mixture methods. *Remote Sensing of Environment*, **47**, 311–321.

GAO, B. C., and GOETZ, A. F. H., 1994, Extraction of dry leaf spectral features from reflectance spectra of green vegetation. *Remote Sensing of Environment*, **47**, 369–374.

GAO, B. C., HEIDELBRECHT, K. B., and GEOTZ, A. F. H., 1993, Derivation of scaled surface reflectance form AVIRIS data. *Remote Sensing of Environment*, **44**, 165–178.

GOETZ, A. F. H., 1991 Imaging spectroscopy of studying Earth, air and water, *EARSel, Advances in Remote Sensing*, **1**, 3–15.

GREEN, A. A., and CRAIG, M. D., 1985, Analysis of aircraft spectrometer data with logarithmic

residuals. *Proceedings of the Airborne Imaging Spectrometer Data Analysis Workshop, JPL Publication* 85-41, Pasadena, California, pp. 111–119.

KAUFMANN, H., WEISBRICH, W., BEYTH, M., BARTOV, Y., ITAMAR, A., MAZOR, E., RONEN, S., and KAFRI, U., 1991, Mineral identification using GER-II data acquired from Makhtesh Ramon/Negev, Israel. *EARsel Advances in Remote Sensing*, **1**, 82–92.

KNEIZYS, F. X., ANDERSON, G. P., SHETTLE, E. P., GALLERY, W. O., ABREU, L. W., SELBY, J. E. A., CHETWYND, G. P., and CLOUGH, S. A., 1988, User guide to *LOWTRAN-7*, Environmental Research Papers No.: 1010: AFGL-TR-88-0177: Air-Force Geophysical Laboratories.

KRUSE, F. A., 1988, Use of airborne imaging spectrometer data to map minerals associated with hydrothermally altered rocks in the northern Grapenvine Mountains, Nevada and California. *Remote Sensing of Environment*, **24**, 31–51.

KRUSE, F. A., KIEREIN-YOUNG, K. S., and BOARDMAN, J. W., 1990, Mineral mapping at Cuperite, Nevada with the 63 channel imaging spectrometer. *Photogrammetric Engineering and Remote Sensing*, **56**, 83–92.

MACKIN, S., and MUNDAY, T. J., 1988, Imaging spectroscopy in environmental science research and applications—preliminary results from the analysis of GER-II imaging spectrometer data—Australia and the USA. Department of Geological Sciences, University of Durham, Durham, England, Interim Report 1, Contract no: D/ER1/9/4/2052/40/RAE(F)BNSC, 44 pp.

RAST, M., HOOK, S. J., ELVIDGE, C. D., and ALLEY, R. C., 1991, An evaluation of techniques for the extraction of mineral absorption features from high spectral resolution remote sensing data. *Photogrammetric Engineering and Remote Sensing*, **57**, 1303–1309.

ROBERTS, D. A., YAMAGUCHI, Y., and LYON, R. J. P., 1985, Calibration of airborne imaging spectrometer data to percent reflectance using field spectral measurements. *Proceedings of the Nineteenth International Symposium on Remote Sensing of Environment, Ann Arbor, Michigan, 21–25 October*. ERIM, Ann Arbor, MI, 679–688.

TANRE, D., DEROO, C., and DUHAUT, P., 1990, Description of a computer code to simulate the satellite signal in the solar spectrum: the 5S code. *International Journal of Remote Sensing*, **11**, 659–668.

WERNER, K., and LEHMANN, F., 1991, EISAC'89: Evaluation of GER airborne scanner data in the Almaden test site (Spain). *EARsel Advances in Remote Sensing*, **1**, 43–47.